Dual Self-Assembled Nanostructures from Intrinsically Disordered Protein Polymers with LCST Behavior and Antimicrobial Peptides

*Sergio Acosta†, Zhou Ye‡, Conrado Aparicio‡, Matilde Alonso† and J. Carlos Rodríguez-Cabello†**

†BIOFORGE (Group for Advanced Materials and Nanobiotechnology), CIBER-BBN, University of Valladolid, 47011 Valladolid, Spain

‡MDRCBB, Minnesota Dental Research Center for Biomaterials and Biomechanics, University of Minnesota, Minneapolis, Minnesota 55455, USA Address here.

E-mail: roca@bioforge.uva.es

KEYWORDS: Self-assembly, antimicrobial peptides, protein polymers, intrinsically disordered proteins, nanomaterials

ABSTRACT

Antimicrobial peptides (AMPs) have attracted great interest as they constitute one of the most promising alternatives against drug-resistant infections. Their amphipathic nature provides them antimicrobial and immunomodulatory properties but also the ability to self-assemble into

supramolecular nanostructures. Here, we propose their use as self-assembling domains to drive hierarchical organization of intrinsically disordered protein polymers (IDPPs). Using a modular approach, hybrid protein-engineered polymers were recombinantly produced, thus combining designer AMPs and a thermoresponsive IDPP, an elastin-like recombinamer (ELR). We exploited the ability of these AMPs and ELRs to self-assemble to develop supramolecular nanomaterials by way of a dual-assembly process. First, the AMPs trigger the formation of nanofibers, then the thermoresponsiveness of the ELRs enables assembly into fibrillar aggregates. The interplay between the assembly of AMPs and ELRs provides an innovative molecular tool in the development of self-assembling nanosystems with potential use for biotechnological and biomedical applications.

TOC graphic

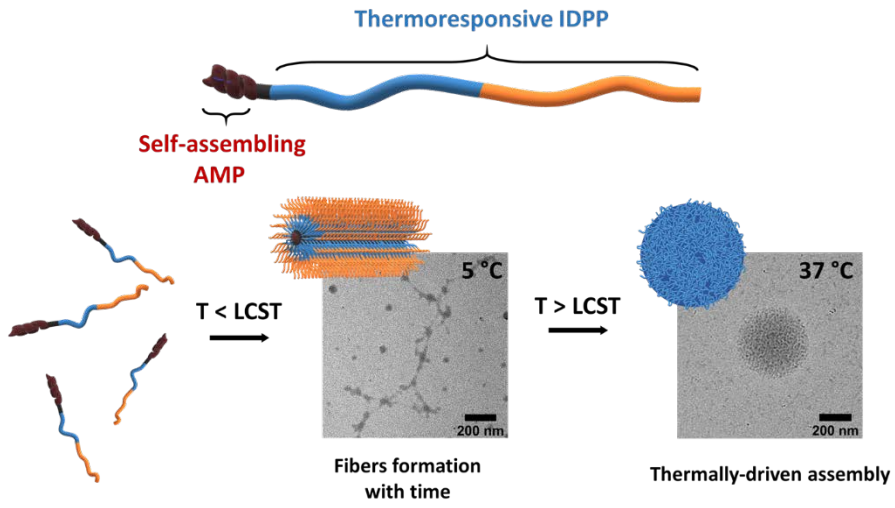

1. Introduction

Self-assembly is ubiquitous in Nature and is a powerful strategy for the fabrication of materials.[1] Understanding the self-assembling processes of biological systems facilitates the fabrication of novel supramolecular materials and vice versa. Proteins, one of the most abundant macromolecule in living systems, constitute an important source of inspiration.[2] Given their multiple and unique functions, as well as their simple composition, protein-inspired materials enable the development of advanced self-assembling nanosystems with virtually limitless variations of their biochemical and bioactive properties for biotechnological and material engineering applications.[3–5] In this sense, proteins that undergo phase transition and organize into hierarchical assemblies have been especially relevant. A common feature of these proteins is the presence of structural disorder. Despite the lack of defined tertiary structure, intrinsically disordered proteins (IDPs) and protein regions (IDRs) are involved in vital cell functions. Indeed, structural disorder plays a fundamental role in the mechanical properties of elastomeric proteins and in protein phase transition.[6,7] A number of IDPs and IDRs phase-separate under physiological conditions driving the formation of subcellular membraneless compartments (so-called biomolecular condensates).[7,8]

Intrinsically disordered protein polymers (IDPPs) are artificial polypeptides composed by the repetition of conserved motifs found in IDRs, typically in structural proteins.[9] This confers them stimuli-responsiveness and valuable mechanical properties that make them interesting candidates for the biofabrication of hierarchical materials.[10] This is the case of elastin-like recombinamers (ELRs), a class of protein-engineered polymers based on low-complexity sequences found in the hydrophobic domains of tropoelastin.[11] ELRs are biocompatible protein polymers that undergo a reversible lower critical solution temperature (LCST) phase transition in aqueous solution.[12] Rational modular approaches lead the synthesis of elastin-like multiblock-copolymers that self-

assemble at physiological temperature into different nanostructures and hydrogels.[10] Moreover, the thermoresponsive self-assembly can be extended further to create more complex architectures. Other self-assembling protein domains can be introduced in the modular design with exquisite control thanks to their recombinant production,[13] thus controlling self-assembly process and giving access to new synthetic designs. As such, IDPPs offer a tailored platform for the fabrication of self-assembling nanosystems for fundamental or applied sciences, including molecular models for IDPs and biomolecular condensates,[14,15] advanced nanovehicles for drug delivery or multifunctional scaffolds for tissue engineering.[16–20] Nevertheless, there is a need for innovative self-assembling domains that expand the range of molecular designs and functionalities of hybrid IDPPs.

Antimicrobial peptides (AMPs) are short (10-50 amino acids) and generally cationic peptides found in a wide variety of multicellular organisms.[21] Natural and designer AMPs have gained increasing attention in recent years due to their broad-spectrum activity and immunomodulatory properties as well as their ability to form supramolecular assemblies.[22,23] Self-assembling behavior results from their amphipathicity, which allows them to interact with several molecular targets.[23–25] Recent studies have demonstrated the possibility to obtain different supramolecular architectures from different AMPs, including fibers,[26] spherical nanoparticles,[27] twisted nanoribbons or hydrogels.[28–32] Additionally, AMPs can be chemically conjugated with synthetic and natural self-assembling polymers or functionalized with peptide amphiphiles in order to enhance their antimicrobial performance.[33–35] However, despite the increasing interest on AMPs and AMP-conjugates, no one to the best of our knowledge has studied their potential as self-assembling domains within protein-engineered polymers.

Herein, this study aims to investigate the interplay of self-assembling AMPs and IDPPs, in this case ELRs. We propose an alternative approach for the design of hierarchically self-assembled nanomaterials that exploits the self-assembly capability of AMPs and the thermoresponsiveness of ELRs. We hypothesized that the recombinant synthesis of hybrid polymers combining AMPs within IDPPs could lead to hierarchical supramolecular assembly by way of a dual process. Thus, self-assembling properties of AMPs could be synergistically combined with the stimuli-responsiveness of the IDPPs in order to fabricate functional supramolecular materials for biotechnological and biomedical applications. De novo designed AMP-ELRs were recombinantly produced and their thermal behavior and self-assembly dynamics were characterized via turbidimetry, circular dichroism (CD) spectroscopy, dynamic light scattering (DLS) and electron microscopy. This approach seeks to shed light on the complex mechanisms that govern the supramolecular assembly of hybrid AMP-IDPP systems, thus setting the basis for the synthesis of advanced bioinspired materials that synergistically combine their complex self-assembly dynamics.

2. Experimental section

2.1. Gene construction

Gene construction of the AMP-IDPPs was performed using previously described procedures.[36] Encoding genes for the AMPs were purchased from NZYTech, Lda. (Portugal) and cloned into a modified pDrive plasmid flanked by *Ear*I restriction sites, using *E. coli* XL-1 blue (Agilent, USA) as cloning strain. The final genetic constructs were then completed using the iterative recursive method.[36]

2.2. Bioproduction and purification

All the protein polymers used in this work were recombinantly bioproduced. Briefly, encoding genes were cloned into pET-25b (+) expression vectors and transformed into *E. coli* BLR (DE3) for heterologous expression. After overnight fermentation in a 15 L bioreactor (Applikon Biotechnology, the Netherlands), the biopolymers were purified taking advantage of the lower critical solution temperature (LCST) phase transition of the ELRs by inverse transition cycling (ITC), adding 1.5 M NaCl for warm precipitation.[36] After three cycles, the biopolymers were found to be pure and monodisperse by SDS-PAGE, and were then dialyzed against ultrapure water, lyophilized and stored at -20 °C. The yields observed ranged from 380 to 600 mg L^{-1} of purified IDPPs (ELR/AMP-ELR) per liter of bacterial culture.

Protective block cleavage and purification. AMP-ELRs were designed and bioproduced in *E. coli* as pro-polypeptides (Table S1). After recombinant expression, the purity of the pro-AMP-ELRs was verified by SDS-PAGE (Figure S1). The sacrificial block was then removed. To that end, pro-polypeptides were incubated with CNBr solution (70% formic acid, FA) at a Met:CNBr molar ratio of 1:200. The reaction was performed for 20 h at room temperature in the darkness and under anaerobic conditions. CNBr was then eliminated on a rotary evaporator. The ELRs were resuspended in ultrapure water and dialyzed. After four dialysis steps against cold ultrapure water and lyophilization, the cleaved AMP-ELR was purified using HisPur™ Ni-NTA resin (ThermoFisher Scientific, USA) following a batch methodology. Briefly, the lyophilized products were dissolved in denaturing buffer (4 M urea, 20 mM sodium phosphate, 500 mM NaCl) in order to prevent physical interactions between the AMPs, mixing 30 mL of the dialyzed solution with 15 mL of the resin in 50 mL tubes and incubating at 200 rpm and 4 °C for 3 h. The resin was then centrifuged. Due to the presence of the His tag, sacrificial block and the uncleaved

copolymers bonded to the resin, whereas the AMP-ELR remained in the supernatant. After two purification steps, AMP-ELRs were completely purified (Figure S2). Finally, the protein polymer solutions were dialyzed, filtered (0.22 μm Nalgene™, ThermoFisher Scientific, USA), lyophilized and stored at -20 °C until further use.

The monodispersity and purity of the hybrid AMP-ELRs were assessed by SDS-PAGE (Figure 1, S2), MALDI-TOF (Table S2 and Figure S3) and HPLC (Table S3). MALDI-TOF and HPLC analysis were performed in the "Laboratorio de Técnicas Instrumentales" (LTI) at the University of Valladolid (Spain).

2.3. Phase transition characterization

The thermal behavior was evaluated by turbidimetry, measuring the absorbance at 350 nm in the range 5-40 °C with a scan step of 0.5 °C using a Cary 100 UV-Vis spectrophotometer (Agilent). Heating and cooling ramps were performed at 0.25 °C min^{-1} while stirring. The T_t were determined as the temperature corresponding to the maximum of the first derivative of the optical density versus temperature and the thermal hysteresis was the difference between the $T_{t\,(heating)}$ and $T_{t\,(cooling)}$. All samples were prepared in ultrapure water at a concentration of 25 μM and measured in triplicate.

2.4. Physical characterization of the nanostructuration

Since ELRs exhibit a LCST phase transition in solution, the self-assembly dynamics of the hybrid protein polymers (AMP-ELRs) were evaluated below and above the transition temperature (T_t) of the ELR. To that end, 25 μM solutions in ultrapure water were prepared under

sterile conditions and incubated at 5 or 37 °C for 10 min, 1 h, 4 h, 1 d, 3 d, and 7 d. Nanostructuration of the ELR/AMP-ELRs was then analyzed by DLS and TEM.

The nanoparticle size distribution was evaluated by DLS using a Zetasizer Nano (Malvern Instruments, UK), with a 173° scattering angle and equipped with a HeNe laser (633 nm) with an output power of 10 mW. Each sample was measured in triplicate.

TEM samples were prepared on 300-mesh carbon-coated copper grids with negative staining. First, grids were rendered hydrophilic by plasma treatment in a PDC-002 plasma cleaner (Harrick Plasma, USA) at a low power setting (7.2 W applied to the RF coil) for 20 s. Then, 15 μL of the pre-incubated polymers, ultrapure water and uranyl acetate (1% w/v) solution were dropped onto a Parafilm® strip over pre-chilled (5 °C) or pre-heated (37 °C) glass surfaces. Plasma treated grids were placed onto the polymer drop for 90 s, on ultrapure water for 60 s, and, finally, on the negative staining solution for another 60 s. Blotting filter paper was used to remove excess solution after every step.

Images were taken using a Tecnai Thermionic T20 microscope operating at 200 kV (SAI, University of Zaragoza, Spain.

2.5. Circular dichroism

ELR or AMP-ELR solutions were prepared at 5 μM in pre-chilled ultrapure water and incubated at 5 or 37 °C for 10 min, 1 h, 4 h, 1 d, 3 d, and 7 d. The CD signal was measured for a 200 μL solution in a quartz cuvette (1 mm path-length) using a CD spectrometer (Jasco J-815, Easton, MD, USA), scanning over a range of 260-190 nm with a data pitch of 1 nm, a scanning

rate of 50 nm min^{-1} and a response time of 2 s. All measurements were subtracted from the background signal from ultrapure water in the quartz cuvette and repeated in triplicate.

2.6. Cryogenic TEM

To test the thermoresponsiveness of the fibrillar structures formed by the AMP-ELRs, nanofibers were preformed and the behavior of the nanostructures evaluated by cryo-TEM. To that end, 25 μM solutions of the three protein-engineered polymers in ultrapure water were incubated at 5 °C for 24 h in order to drive the AMP fibrillar assembly. Samples were then heated at 37 °C for 30 min. Cryo-TEM samples were prepared before and after heating to evaluate changes in the nanostructuration, as well as DLS measurements were performed.

Preparation and visualization of the cryo-TEM samples was carried out at the Electron Microscopy Platform (CICbioGUNE, University of the Basque Country, Spain). To that end, four microliters of the sample were placed onto a glow-discharged 300-mesh lacey-carbon coated grid (Lacey Carbon film on 300 mesh copper; LC300-Cu; Electron Microscopy Sciences) and incubated inside the chamber of a Vitrobot Mark III (FEI Inc., The Netherlands) at 4 °C and at a relative humidity close to saturation (95% RH) for 30 s. Most of the liquid in the grid was removed by blotting (3 s at an offset of -3 mm) and vitrified by plunging into liquid ethane, previously cooled with liquid nitrogen at approximately -180 °C.

Images were collected at liquid nitrogen temperature using a JEM-2200FS/CR (JEOL Europe, Croissy-sur-Seine, France) field emission gun transmission electron microscope operating at 200 kV. An in-column energy filter (Omega filter) produced images with improved contrast and signal-to-noise ratio by zero-loss filtering. The energy slit width was set to 15 eV. Digital images

were recorded using a 4K × 4K Ultrascan4000™ charge-coupled device (CCD) camera (Gatan, Inc.) running DigitalMicrograph™ (Gatan, Inc.) software.

3. Results and discussion

3.1. Molecular design and bioproduction of AMP-ELR protein polymers

Hybrid protein polymers were engineered and biosynthesized by recombinant DNA technology using a modular design in which two different domains can be differentiated (AMP and ELR, Figure 1a). We chose ELRs as model IDPP because they mimic the physicochemical and biological properties of tropoelastin.[37] ELRs exhibit intrinsic molecular disorder, tunable LCST phase behavior and biocompatibility. Moreover, ELRs have been shown to be useful as purification tags for the expression of different proteins and peptides,[38] including AMPs,[39,40] in high yield, thus resulting in a variety of possibilities for supramolecular assembly.[41–43] In this approach, we employed an ELR, referred to as SI, with amphiphilic diblock design. The SI protein polymer (ELR control) contains the hydrophilic S-block [(Val-Pro-Gly-Ser-Gly)$_{50}$] and the hydrophobic I-block [(Ile-Pro-Gly-Val-Gly)$_{60}$], which have LCSTs below and above physiological temperature, respectively.[44] At 37 °C, the hydrophobic block (I) collapses into hydrophobic cores surrounded by a hydrophilic corona (S), thus driving the formation of micellar nanostructures (schematically represented in Figure 1c). The AMP was located at the N-terminus, connected to the hydrophilic block (S) via a flexible poly-Gly spacer. This meant that both potential self-assembling domains (SADs), namely the AMP and the hydrophobic block of the ELR, were located at opposite ends of the molecule (Figure 1a). For AMPs, we chose the well-characterized designer peptides GL13K and 1018.[45,46] These AMPs have similar molecular properties (i.e. number of amino acids, charge, hydrophobicity, and hydrophobic moment)[47] and both have been shown to self-assemble in solution.[28,48]

AMP-ELRs were produced as pro-polypeptides by introducing a sacrificial ELR block, referred to as HE, at the N-terminus of the AMP-ELR construct (Table S1). This block plays a key role during bioproduction because: a) it protects the host bacterial strain from the toxic side-effects of the AMP during fermentation; b) it increases the expression levels; c) it enables site-specific cleavage. A Met was incorporated at the C-terminus to allow us to release the AMP-ELRs with no extra amino acid that may affect their bioactivities; and d) it facilitates purification of the AMP-ELR with a designed histidine tag intended for selective removal of the HE block and the uncleaved products from the AMP-ELRs.

After recombinant production, inverse transition cycling (ITC) purification and chemical cleavage of the sacrificial block, AMP-ELRs were purified on a nickel-charged agarose resin (Figure S1 and S2). Monodisperse and highly pure products were obtained, as revealed by sodium dodecyl sulfate–polyacrylamide gel electrophoresis (SDS-PAGE), matrix-assisted laser desorption/ionization time-of-flight (MALDI-TOF) mass spectrometry and high performance liquid chromatography (HPLC) analysis (Figure 1b, S3 and Table S2, S3).

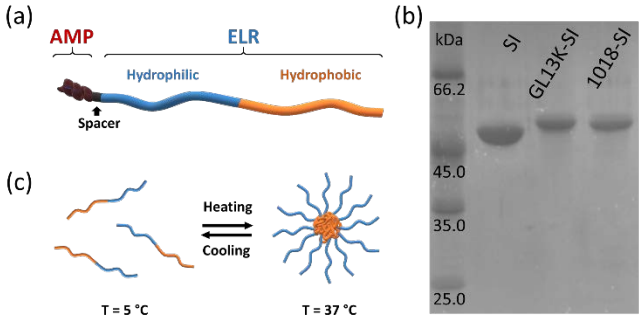

Figure 1. (a) Molecular scheme of the modular design of the hybrid protein polymers (AMP-ELRs). Individual blocks (AMP, spacer and ELR) are not to scale. Additional information regarding the molecular weights can be found in the Supporting Information. (b) Copper-stained SDS-PAGE of the pure recombinant products: SI ELR and the hybrid AMP-ELRs (GL13K-SI and 1018-SI). (c) Scheme of the thermally-driven self-assembly of the ELR control, SI, into spherical micelles.

3.2. **Thermal behavior characterization**

Given the thermosensitivity of the ELRs, we studied the thermal behavior of the hybrid AMP-ELRs in aqueous solution by monitoring the evolution of the optical density at 350 nm (OD^{350}) during consecutive heating and cooling cycles in the range 5-40 °C (Figure 2 and S4). All three protein-engineered polymers (SI, GL13K-SI and 1018-SI) showed a reversible LCST phase transition with thermal hysteresis and a transition temperature (T_t) below physiological temperature (Table 1). Additionally, a slight increase in the OD^{350} after cooling the samples was observed. This may indicate that the process is not completely reversible. SI polypeptides were soluble below T_t. Upon increasing the temperature above the T_t, collapse of the I-block triggered the formation of hydrophobic cores, which were stabilized in solution by surrounding hydrophilic coronas (S-blocks), thus meaning that SI self-assembled into micellar nanostructures.[44] When the samples were cooled, these micelles disassembled and the OD^{350} decreased. However, a minimal fraction of the hydrophobic interactions between isoleucine side-chains seemed to remain, thus meaning that disassembly was not completely reversible. Consequently, OD^{350} was slightly greater than prior to heating, progressively increasing after each consecutive heating-cooling cycle (Figure S4). Furthermore, and consistent with previous studies with the IDPP analogs poly(Val-Pro-Gly-Leu-Gly),[49] thermal hysteresis was observed during cooling cycles, possibly as a result of these hydrophobic interactions.

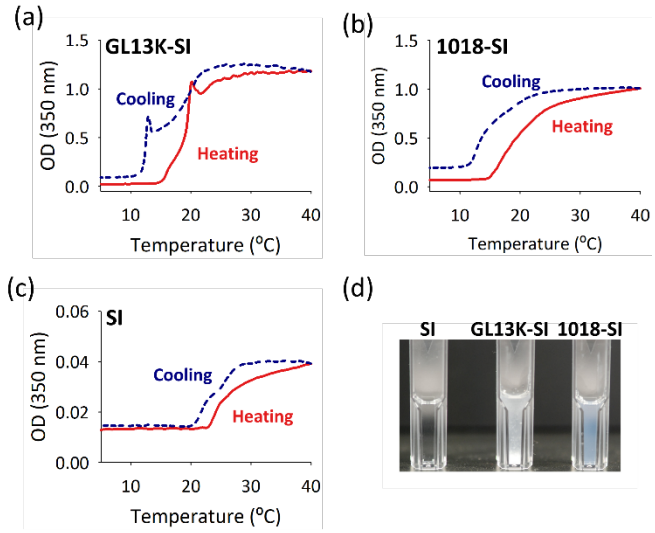

Figure 2. Thermal behavior of the hybrid AMP-ELRs (a, b) and the ELR (c) monitored by turbidimetry. (d) Images of the protein polymer solutions at 37 °C (25 μM in ultrapure water). Evolution of optical density (OD) as a function of temperature demonstrated that all protein polymers exhibit a reversible phase transition. The presence of AMPs contributed to the phase transition and thermal hysteresis. Solid red lines represent heating cycles and dashed blue lines represent cooling ones.

Similarly, hybrid AMP-ELRs also underwent a quasi-reversible phase transition, although with substantial differences (Figure 2). SI self-assembles into stable nanostructures in solution and, as a consequence, the OD^{350} is less than 0.05. In contrast, for the hybrid AMP-ELRs, OD^{350} was much higher at temperatures above T_t. As observed previously for AMPs in solution,[28,48] AMP domains can self-interact and may assemble into larger aggregates, thus increasing the OD^{350}. Moreover, divergences were observed between the turbidity profiles of the hybrid protein polymers. Whereas 1018-SI showed a thermal behavior similar to the ELR control (SI), GL13K-SI underwent a sharper transition with a peak, which suggested that GL13K tendency to fold may alter the assembly process of the ELR.

The presence of AMP affected the phase transition when compared with the SI polymer, thus suggesting a cooperative effect in the assembly (Table 1). The T_t of the hybrid polymers decreased in comparison with the ELR control, which indicates that the interactions between the AMPs favor the cooperative phase transition of the ELR. Similarly, the AMP domains also

enhanced thermal hysteresis. Aggregation of the GL13K and 1018 peptides is associated with the formation of secondary β structures,[47] which would increase the intermolecular order in the coacervate state and, therefore, the hysteresis (Table 1). This behavior is consistent with previous studies in which order-promoting domains (e.g., poly-Ala) were introduced into the IDPP backbone.[20] Besides that, coacervation of the ELR-domain seemed to promote the assembly of the AMPs. After heating-cooling cycling, the OD^{350} of the AMP-ELR samples gradually increased (Figure S4a and S4b) and this increase was substantially greater comparing with the control (SI), which also evidenced the synergy between the AMP and the ELR domains in the assembly of the hybrid protein polymers.

Table 1. Transition temperatures (T_t) and hysteresis (ΔT_t) of the ELR (SI) and the hybrid AMP-ELRs (GL13K-SI and 1018-SI).

	SI	**GL13K-SI**	**1018-SI**
T_t heating	23.6±0.4	19.6±0.5	17.5±0.6
T_t cooling	21.7±0.3	13.0±0.6	13.1±0.4
Hysteresis (ΔT_t)	1.9±0.3	6.6±0.3	4.5±0.4

3.3. Self-assembly dynamics

Phase-transition characterization suggested that the AMP domains may play an important role in the supramolecular assembly of AMP-ELRs by contributing to the formation of aggregates of higher order complexity than micellar assemblies and stabilization of the assembled structure, thus increasing thermal hysteresis. As such, we proceeded to characterize the self-assembly dynamics below and above T_t of the I-block in detail.

At 5 °C (below T_t), ELR molecules were completely soluble, and the ELR control (SI) did not form any nanostructures (Figure 3 and 4a). Moreover, a DLS distribution of around 10 nm corresponds to the value for soluble macromolecules.[50] In contrast, the presence of AMPs within the recombinant polymers triggers self-assembly into fibrillar nanostructures.

Supramolecular assembly of the peptides 1018 and GL13K has been previously observed in solution, although they require alkaline conditions or the presence of salts to self-assemble.[28,48] Electrostatic repulsion between the positively charged side-groups has to be overcome to favor interaction between the peptides and the formation of higher-order assemblies. Interestingly, in our case, self-assembly of the hybrid protein polymers occurred in salt-free solution (i.e. ultrapure water). Consistently with the thermal characterization, these results suggest that the combination of a larger amphipathic polypeptide chain (i.e. SI) with the AMP may induce a cooperative effect that facilitates aggregation of the AMP domains.

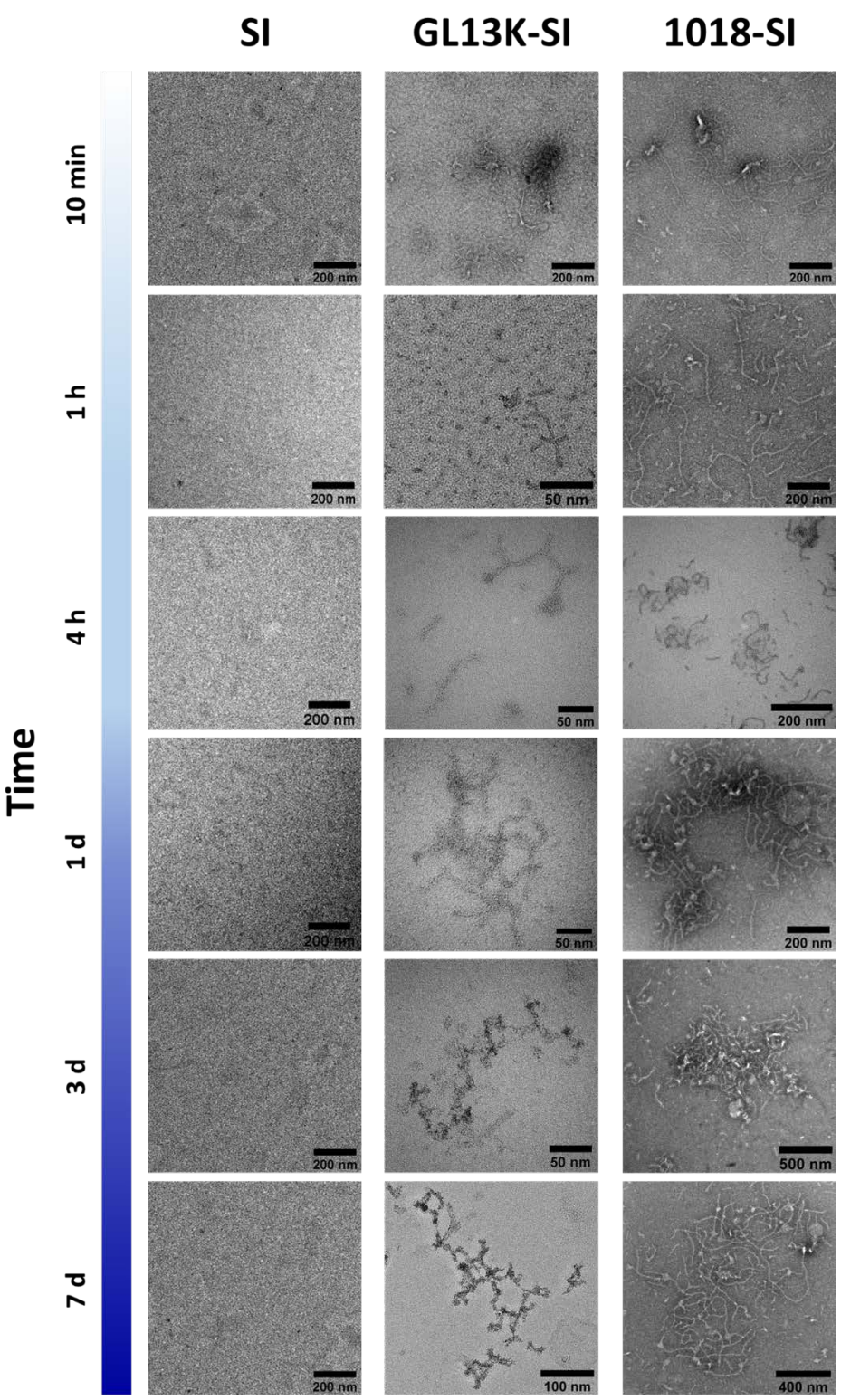

Figure 3. Negatively stained transmission electronic microscopy (TEM) micrographs of the ELR/AMP-ELRs after incubation at 5 °C. Presence of the AMPs drove the formation of nanofibers after short incubation periods (10 min, 1 h) which evolved over time, thus indicating a dynamic behavior.

The fibrillar nanostructures formed by the AMP-ELRs exhibited a dynamic behavior in solution. Although the nanofibers evolved over time in both cases, different aggregation patterns could be observed for each hybrid protein polymer, with 1018-SI forming longer nanofibers than GL13K-SI, as shown by TEM (Figure 3, middle and right column). The growth of GL13K-SI nanofibers seems to be spatially constrained, thus limiting fiber elongation in favor of nanofibers with repeated patterns. DLS analysis showed that despite intensity size distributions of both hybrid polymers overlapped, the nanostructures formed by the 1018-SI polymer were bigger than those formed by GL13K-SI.

In addition to DLS and TEM characterization, structural studies of the hybrid protein polymers were performed using circular dichroism (CD) spectroscopy (Figure S6). Nevertheless, the CD spectra for all polymers were very similar at the different time points below T_t, with a negative peak at ≈197 nm and a weak positive shoulder near 220 nm that are characteristic for unordered polypeptides.[51] The overwhelmingly higher molecular weight of the ELRs compared to the AMP in the ELR-AMP molecules (46 kDa versus ≈1.5 kDa) dominated the CD signal and only minor differences in ellipticity of the 197 nm peak were detected.

In parallel, we also studied the nanostructuration at physiological temperature and found that, above T_t, the I-block underwent a phase transition, thus leading to the formation of defined nanostructures. These micellar assemblies were observed in the three protein polymers after

short incubation periods (10 min, 1 h and 4 h). However, in the hybrid AMP-ELRs, micellar populations coexisted with small nanofibers similar to those observed below T_t (Figure 5).

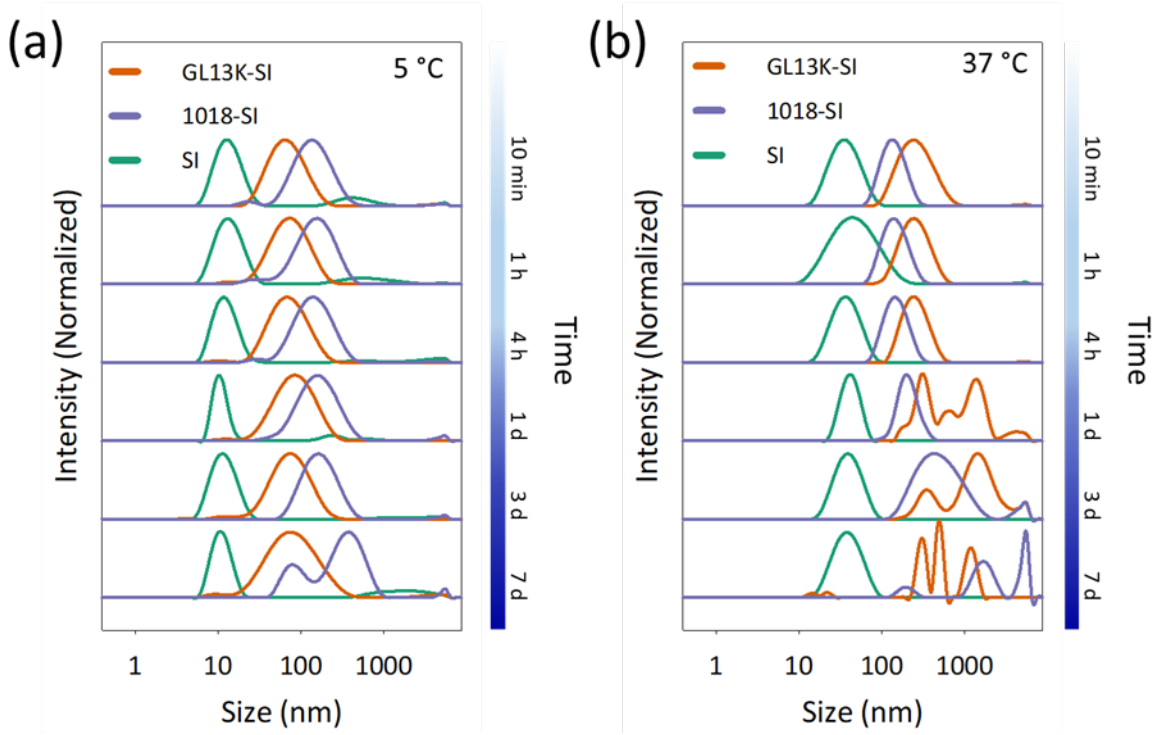

Figure 4. DLS intensity distributions of the three protein-engineered polymers below (a, 5 °C) and above (b, 37 °C) the T_t.

The assembly of the elastin-like hydrophobic block correlated with shift in secondary structure (Figure S6). In the three CD spectra appeared a lower proportion of random coil (minimum at 197 nm) comparing with the spectra below T_t. and a higher proportion of type II β-turns and distorted β-sheets conformations (maximum at ≈210 nm and pronounced minimum at 220 nm), that are characteristic in ELRs.[52,53] In addition, the presence of the AMP in the hybrid polymers resulted in a substantial decrease in the intensity of the random coil peak (197 nm), thus confirming that the presence of the AMP induced an increase of structural order in the hybrid polymers comparing with the SI polymer. It must also be noted that after 1 day of incubation at

37 °C, CD signals of 1018-SI decreased significantly, probably due to the phase separation and the consequent precipitation of the aggregates.

The SI polymer self-assembled into stable and monodisperse micellar nanostructures (hydrodynamic diameter (D_h) = 35.5 nm, polydispersity index (PdI) = 0.125, after 1 week at 37 °C). In contrast, the presence of the AMP in the hydrophilic corona induced the aggregation of the micelles, thus driving a secondary self-assembly in the hybrid protein polymers (Figure 4b). After one incubation day above T_t, AMP-ELRs formed larger aggregates based on interconnected fibers that showed a continuous growth until precipitation. Consistent with the characterization below T_t, the supramolecular assemblies varied depending on the AMP, with different shapes being observed. GL13K-SI preferably formed spherical aggregates while 1018-SI aggregates were more elongated with undefined shapes (Figure 4b and 5).

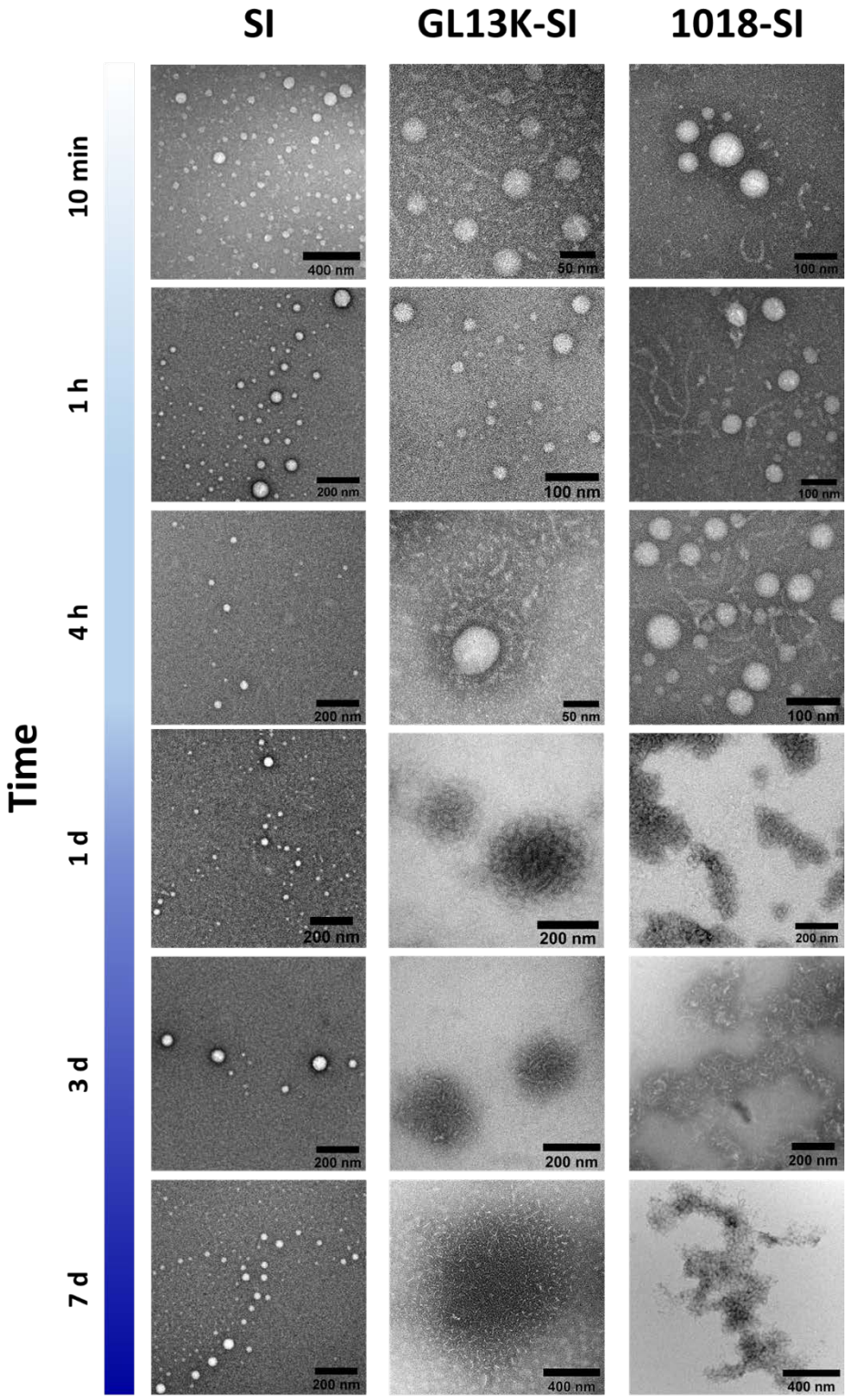

Figure 5. Negatively stained TEM micrographs of the ELR/AMP-ELRs after incubation at 37 °C. The presence of the AMP drives a second self-assembly, which triggers the formation of hierarchical structures. Fibrillar aggregates with globular or amorphous shapes are found when the GL13K or the 1018 peptide, respectively, are found within the hybrid polypeptide.

Both AMPs have similar molecular properties, which may suggest similar self-assembly mechanisms, even though their self-assembly dynamics are substantially different. The different spatial distribution of the charged and hydrophobic residues in the AMPs seems to modulate the driving forces for peptide aggregation, thus meaning that 1018 promotes the formation of longer fibers than GL13K. In this regard, recent studies have demonstrated the divergence of the aggregation tendencies of both peptides. Although both mechanisms of aggregation are pH-dependent, the tendency to acquire β-sheet conformations in solution is greater in 1018 peptide than GL13K at the same pH.[47] GL13K self-assembly requires pH values of 9.6 or greater,[28,54] whereas the tendency of 1018 to aggregate is noticeable from pH values greater than 2, and is highly influenced by the presence of anions.[48] Additionally, it must be noted that the C-terminal conjugation of the peptides with the IDPP chain implicitly introduces steric effects that may affect the assembly process. Interestingly, the diverse tendencies of both AMPs to self-assemble in solution seemed to be affected differently. GL13K peptides tendency to form twisted nanoribbons in solution seemed to be hampered in the hybrid polymer, thus resulting in the formation of nanostructured patterns below T_t (Figure 3). In contrast, bioconjugation of the 1018 with the IDPP seemed to contribute to enhance the spatial self-organization of the peptide, which enabled the formation of fibrillar nanostructures below T_t (Figure 3).

3.4. Thermoresponsive nanostructures

Additionally, we evaluated whether the fibrillary nanostructures formed upon self-assembly of the AMPs retained the LCST behavior of the ELRs. To that end, we incubated the ELR/AMP-ELR solutions at 5 °C for 24 h to pre-form the nanofibers, then carried out a second incubation at physiological temperature for 30 min to assess the influence of temperature on the

nanostructuration. Samples were analyzed via DLS and cryogenic transmission electron microscopy (cryo-TEM) visualization after each incubation (Figure 6 and S7).

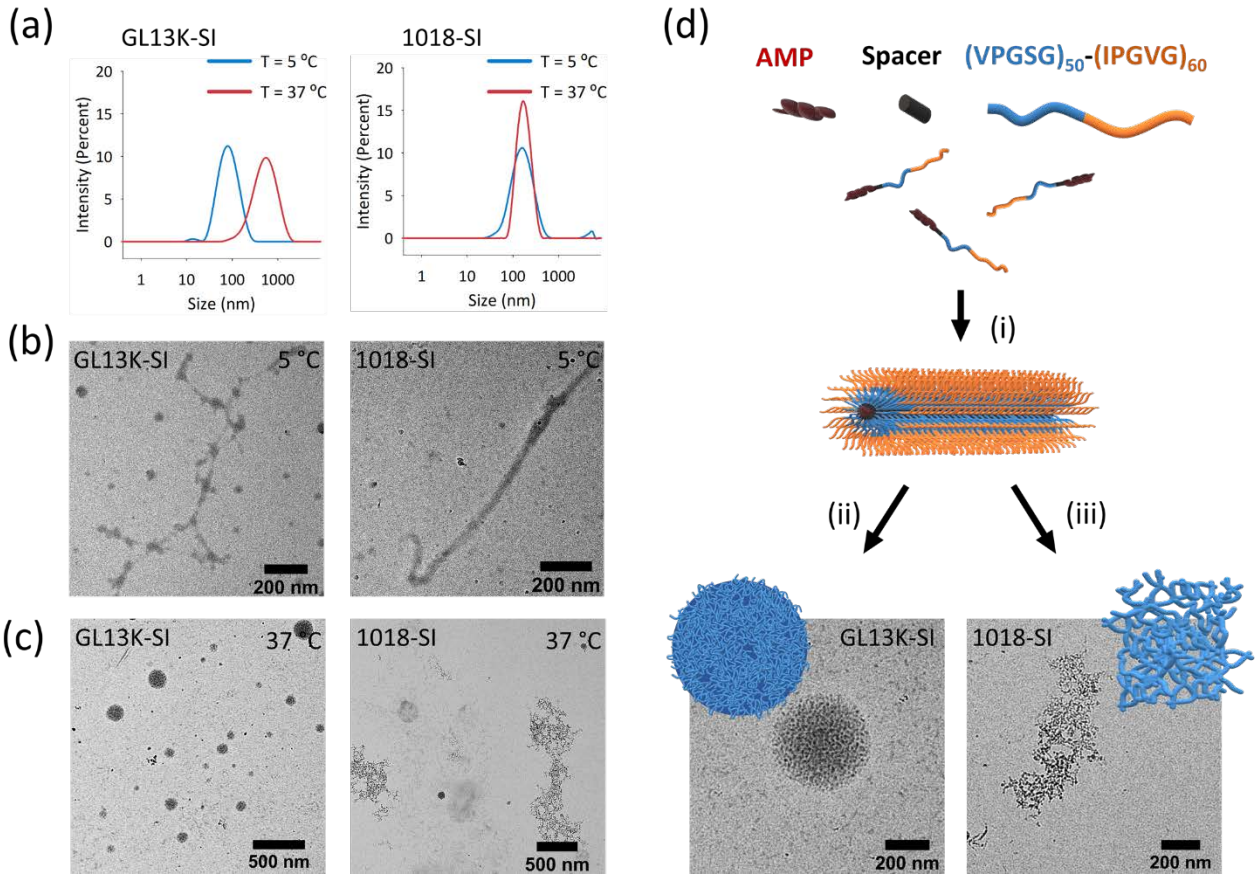

Figure 6. (a) Intensity size distributions of the nanostructures formed by the hybrid protein polymers after the incubation below (5 °C) and above (37 °C) the T_t. (b) Cryo-TEM micrographs of the GL13K-SI and 1018-SI samples after initial incubation at 5 °C for 24 h, where the AMP triggered fibrillar assembly, and (c) after subsequent incubation at 37 °C, where thermally-triggered coacervation of the ELR drove aggregate formation. (d) Schematic representation of the hierarchical self-assembly of the hybrid polymers (AMP-ELR) and magnification of the nanostructures formed at physiological temperature after the incubation at 5 °C.

As expected, incubation below T_t allowed AMP domains to drive the supramolecular assembly of the hybrid polypeptides into nanofibers (Figure 6a and 6b). A subsequent second incubation at physiological temperature induced coacervation of the hydrophobic block of the ELR (I-block), thus exposing the hydrophilic ELR block (S-block). Nanofibers aggregated into fibrillar networks with spherical or undefined shapes, depending on the AMP (Figure 6c). Additionally, the presence of the spacer between the AMP domain and the ELR diblock does not compromise

hierarchical assembly, which suggests that functional spacers, including sequences sensitive to biological or physical stimuli (e.g. protease degradation or pH), may be included in the system. Therefore, we have demonstrated both the ability of AMPs to self-assemble and induce the supramolecular structuration of larger protein-polymers, and that the thermosensitivity of the ELRs is maintained in the fibrillar assembly. These results suggest that AMPs act as order promoting domains in the hybrid protein polymers, thus inducing thermal hysteresis and controlling the supramolecular assembly of the ELR-domain below and above T_t. Recent studies have evidenced that ordered domains highly modulate the hierarchical assembly of the IDPPs into complex architectures.[20,55] In this regard, the synergistic combination of AMPs and IDPPs opens up a wide range of possibilities for the fabrication of hierarchical nanomaterials with advanced functionalities for biotechnology and biomedical engineering.

Lastly, it is important to note that we used this modular approach in order to recognize the identity and properties of the individual building blocks in the hybrid construction. However, further re-engineering of the design would be needed for their future application. As such, our system can be easily modified to enable optimization for the intended application thanks to its recombinant nature. In the light of these results, the AMP-domains were likely to be hidden inside the fibrillar nanostructures. This effect might limit the antimicrobial activity of the assembly but also might be useful for designing nanovehicles or nanoreservoirs that protect the AMP from the environment or three-dimensional scaffolds for tissue engineering applications.

4. Conclusions

The combined use of AMPs with stimuli-responsive protein polymers is a promising strategy for the design of self-assembled nanomaterials for biotechnological and biomedical applications.

We have shown that AMPs can be used as SADs to trigger the assembly of larger IDPPs, with different nanostructures being achieved depending on the AMP. Moreover, their combination with thermoresponsive protein polymers in modular designs enables the manufacture of hierarchical architectures formed by a dual assembly process.

Consequently, our nanosystem represents a sound strategy for the fabrication of smart biomaterials incorporating AMPs. Their recombinant nature facilitates edition of the modular design and the incorporation of other bioactive motifs with extreme control, in addition to a scalable method for their sustainable production and potential widespread use. This investigation provides a new insight into the protein engineering of self-assembling materials that combine the properties of IDPPs and AMPs in a synergistic manner.

Supporting information

Molecular weights and complete sequence of the protein-engineered polymers (Table S1), SDS-PAGE electrophoresis (Figure S1 and S2), MALDI-TOF spectra and results (Figure S3 and Table S2), amino acid composition by HPLC (Table S3), turbidimetry data (Figure S4), DLS correlation functions (Figure S5), CD spectra (Figure S6), DLS and cryoTEM characterization of the SI protein polymer (Figure S7). (PDF)

Acknowledgements

Authors would like to acknowledge the use of 'Servicio General de Apoyo a la Investigación-SAI', University of Zaragoza (Spain). Parts of this work were carried out in the University of Minnesota I.T. Characterization Facility, which receives partial support from NSF through the MRSEC program. The authors are grateful for the funding from the Spanish Government (MAT2016-78903-R, RTI2018-096320-B-C22), Junta de Castilla y León (VA317P18), Interreg

V A España Portugal POCTEP (0624_2IQBIONEURO_6_E) and Centro en Red de Medicina Regenerativa y Terapia Celular de Castilla y León. This research was also supported by the National Institutes of Health's National Center for Advancing Translational Sciences [Translational Research Development Program-TRDP award to Z.Y. from grant UL1TR002494]. The content is solely the responsibility of the authors and does not necessarily represent the official views of the National Institutes of Health's National Center for Advancing Translational Sciences.

References

(1) Zhang, S. Fabrication of Novel Biomaterials through Molecular Self-Assembly. *Nature Biotechnology*. Nature Publishing Group October 1, 2003, pp 1171–1178. https://doi.org/10.1038/nbt874.

(2) Whitesides, G. M. Bioinspiration: Something for Everyone. *Interface Focus* **2015**, *5* (4), 20150031. https://doi.org/10.1098/rsfs.2015.0031.

(3) Luo, Q.; Hou, C.; Bai, Y.; Wang, R.; Liu, J. Protein Assembly: Versatile Approaches to Construct Highly Ordered Nanostructures. *Chemical Reviews*. American Chemical Society November 23, 2016, pp 13571–13632. https://doi.org/10.1021/acs.chemrev.6b00228.

(4) Okesola, B. O.; Mata, A. Multicomponent Self-Assembly as a Tool to Harness New Properties from Peptides and Proteins in Material Design. *Chem. Soc. Rev* **2018**, *47*, 3721. https://doi.org/10.1039/c8cs00121a.

(5) Acar, H.; Srivastava, S.; Chung, E. J.; Schnorenberg, M. R.; Barrett, J. C.; LaBelle, J. L.; Tirrell, M. Self-Assembling Peptide-Based Building Blocks in Medical Applications. *Adv.*

Drug Deliv. Rev. **2017**, *110–111*, 65–79. https://doi.org/10.1016/J.ADDR.2016.08.006.

(6) Rauscher, S.; Pomès, R. Structural Disorder and Protein Elasticity. *Adv. Exp. Med. Biol.* **2012**, *725*, 159–183. https://doi.org/10.1007/978-1-4614-0659-4_10.

(7) Shin, Y.; Brangwynne, C. P. Liquid Phase Condensation in Cell Physiology and Disease. *Science (80-.).* **2017**, *357* (6357), eaaf4382. https://doi.org/10.1126/science.aaf4382.

(8) Banani, S. F.; Lee, H. O.; Hyman, A. A.; Rosen, M. K. Biomolecular Condensates: Organizers of Cellular Biochemistry. *Nat. Rev. Mol. Cell Biol.* **2017**, *18* (5), 285–298. https://doi.org/10.1038/nrm.2017.7.

(9) Dzuricky, M.; Roberts, S.; Chilkoti, A. Convergence of Artificial Protein Polymers and Intrinsically Disordered Proteins. *Biochemistry* **2018**, *57* (17), 2405–2414. https://doi.org/10.1021/acs.biochem.8b00056.

(10) Saha, S.; Banskota, S.; Roberts, S.; Kirmani, N.; Chilkoti, A. Engineering the Architecture of Elastin-Like Polypeptides: From Unimers to Hierarchical Self-Assembly. *Adv. Ther.* **2020**, *3* (3), 1900164. https://doi.org/10.1002/adtp.201900164.

(11) Acosta, S.; Quintanilla-Sierra, L.; Mbundi, L.; Reboto, V.; Rodríguez-Cabello, J. C. Elastin-Like Recombinamers: Deconstructing and Recapitulating the Functionality of Extracellular Matrix Proteins Using Recombinant Protein Polymers. *Adv. Funct. Mater.* **2020**, 1909050. https://doi.org/10.1002/adfm.201909050.

(12) Meyer, D. E.; Chilkoti, A. Quantification of the Effects of Chain Length and Concentration on the Thermal Behavior of Elastin-like Polypeptides. *Biomacromolecules* **2004**, *5* (3), 846–

851. https://doi.org/10.1021/bm034215n.

(13) Jang, Y.; Champion, J. A. Self-Assembled Materials Made from Functional Recombinant Proteins. *Acc. Chem. Res.* **2016**, *49* (10), 2188–2198. https://doi.org/10.1021/acs.accounts.6b00337.

(14) Simon, J. R.; Eghtesadi, S. A.; Dzuricky, M.; You, L.; Chilkoti, A. Engineered Ribonucleoprotein Granules Inhibit Translation in Protocells. *Mol. Cell* **2019**, *75* (1), 66-75.e5. https://doi.org/10.1016/j.molcel.2019.05.010.

(15) Lecommandoux, S.; Zhao, H.; Ibrahimova, V.; Garanger, E. Dynamic Spatial Formation and Distribution of Intrinsically Disordered Protein Droplets in Macromolecularly Crowded Protocells. *Angew. Chemie Int. Ed.* **2020**. https://doi.org/10.1002/anie.202001868.

(16) Mozhdehi, D.; Luginbuhl, K. M.; Simon, J. R.; Dzuricky, M.; Berger, R.; Varol, H. S.; Huang, F. C.; Buehne, K. L.; Mayne, N. R.; Weitzhandler, I.; et al. Genetically Encoded Lipid–Polypeptide Hybrid Biomaterials That Exhibit Temperature-Triggered Hierarchical Self-Assembly. *Nat. Chem.* **2018**, *10* (5), 496–505. https://doi.org/10.1038/s41557-018-0005-z.

(17) Jang, Y.; Choi, W. T.; Heller, W. T.; Ke, Z.; Wright, E. R.; Champion, J. A. Engineering Globular Protein Vesicles through Tunable Self-Assembly of Recombinant Fusion Proteins. *Small* **2017**, *13* (36), 1700399. https://doi.org/10.1002/smll.201700399.

(18) van Eldijk, M. B.; Schoonen, L.; Cornelissen, J. J. L. M.; Nolte, R. J. M.; van Hest, J. C. M. Metal Ion-Induced Self-Assembly of a Multi-Responsive Block Copolypeptide into Well-Defined Nanocapsules. *Small* **2016**, *12* (18), 2476–2483.

https://doi.org/10.1002/smll.201503889.

(19) Gonzalez, M. A.; Simon, J. R.; Ghoorchian, A.; Scholl, Z.; Lin, S.; Rubinstein, M.; Marszalek, P.; Chilkoti, A.; López, G. P.; Zhao, X. Strong, Tough, Stretchable, and Self-Adhesive Hydrogels from Intrinsically Unstructured Proteins. *Adv. Mater.* **2017**, *29* (10), 1604743. https://doi.org/10.1002/adma.201604743.

(20) Roberts, S.; Harmon, T. S.; Schaal, J. L.; Miao, V.; Li, K.; Hunt, A.; Wen, Y.; Oas, T. G.; Collier, J. H.; Pappu, R. V.; et al. Injectable Tissue Integrating Networks from Recombinant Polypeptides with Tunable Order. *Nat. Mater.* **2018**, *17* (12), 1154–1163. https://doi.org/10.1038/s41563-018-0182-6.

(21) Hancock, R. E. W.; Sahl, H. G. Antimicrobial and Host-Defense Peptides as New Anti-Infective Therapeutic Strategies. *Nat. Biotechnol.* **2006**, *24* (12), 1551–1557. https://doi.org/10.1038/nbt1267.

(22) Bechinger, B.; Gorr, S.-U. Antimicrobial Peptides: Mechanisms of Action and Resistance. *J. Dent. Res.* **2017**, *96* (3), 254–260. https://doi.org/10.1177/0022034516679973.

(23) Torres, M. D. T.; Sothiselvam, S.; Lu, T. K.; de la Fuente-Nunez, C. Peptide Design Principles for Antimicrobial Applications. *Journal of Molecular Biology*. Academic Press August 23, 2019, pp 3547–3567. https://doi.org/10.1016/j.jmb.2018.12.015.

(24) Hale, J. D.; Hancock, R. E. Alternative Mechanisms of Action of Cationic Antimicrobial Peptides on Bacteria. *Expert Rev. Anti. Infect. Ther.* **2007**, *5* (6), 951–959. https://doi.org/10.1586/14787210.5.6.951.

(25) Mansour, S. C.; Pena, O. M.; Hancock, R. E. W. Host Defense Peptides: Front-Line Immunomodulators. *Trends Immunol.* **2014**, *35* (9), 443–450. https://doi.org/10.1016/j.it.2014.07.004.

(26) Liu, Y.; Yang, Y.; Wang, C.; Zhao, X. Stimuli-Responsive Self-Assembling Peptides Made from Antibacterial Peptides. *Nanoscale* **2013**, *5* (14), 6413–6421. https://doi.org/10.1039/c3nr00225j.

(27) Goel, R.; Garg, C.; Gautam, H. K.; Sharma, A. K.; Kumar, P.; Gupta, A. Fabrication of Cationic Nanostructures from Short Self-Assembling Amphiphilic Mixed α/β-Pentapeptide: Potential Candidates for Drug Delivery, Gene Delivery, and Antimicrobial Applications. *Int. J. Biol. Macromol.* **2018**, *111*, 880–893. https://doi.org/10.1016/j.ijbiomac.2018.01.079.

(28) Ye, Z.; Zhu, X.; Acosta, S.; Kumar, D.; Sang, T.; Aparicio, C. Self-Assembly Dynamics and Antimicrobial Activity of All l- and d-Amino Acid Enantiomers of a Designer Peptide. *Nanoscale* **2019**, *11* (1), 266–275. https://doi.org/10.1039/c8nr07334a.

(29) Baral, A.; Roy, S.; Ghosh, S.; Hermida-Merino, D.; Hamley, I. W.; Banerjee, A. A Peptide-Based Mechano-Sensitive, Proteolytically Stable Hydrogel with Remarkable Antibacterial Properties. *Langmuir* **2016**, *32* (7), 1836–1845. https://doi.org/10.1021/acs.langmuir.5b03789.

(30) Jiang, L.; Xu, D.; Sellati, T. J.; Dong, H. Self-Assembly of Cationic Multidomain Peptide Hydrogels: Supramolecular Nanostructure and Rheological Properties Dictate Antimicrobial Activity. *Nanoscale* **2015**, *7* (45), 19160–19169.

https://doi.org/10.1039/c5nr05233e.

(31) Veiga, A. S.; Sinthuvanich, C.; Gaspar, D.; Franquelim, H. G.; Castanho, M. A. R. B.; Schneider, J. P. Arginine-Rich Self-Assembling Peptides as Potent Antibacterial Gels. *Biomaterials* **2012**, *33* (35), 8907–8916. https://doi.org/10.1016/J.BIOMATERIALS.2012.08.046.

(32) Nandi, N.; Gayen, K.; Ghosh, S.; Bhunia, D.; Kirkham, S.; Sen, S. K.; Ghosh, S.; Hamley, I. W.; Banerjee, A. Amphiphilic Peptide-Based Supramolecular, Noncytotoxic, Stimuli-Responsive Hydrogels with Antibacterial Activity. *Biomacromolecules* **2017**, *18* (11), 3621–3629. https://doi.org/10.1021/acs.biomac.7b01006.

(33) Sun, H.; Hong, Y.; Xi, Y.; Zou, Y.; Gao, J.; Du, J. Synthesis, Self-Assembly, and Biomedical Applications of Antimicrobial Peptide–Polymer Conjugates. *Biomacromolecules* **2018**, *19* (6), 1701–1720. https://doi.org/10.1021/acs.biomac.8b00208.

(34) Chang, R.; Subramanian, K.; Wang, M.; Webster, T. J. Enhanced Antibacterial Properties of Self-Assembling Peptide Amphiphiles Functionalized with Heparin-Binding Cardin-Motifs. *ACS Appl. Mater. Interfaces* **2017**, *9* (27), 22350–22360. https://doi.org/10.1021/acsami.7b07506.

(35) Lombardi, L.; Shi, Y.; Falanga, A.; Galdiero, E.; de Alteriis, E.; Franci, G.; Chourpa, I.; Azevedo, H. S.; Galdiero, S. Enhancing the Potency of Antimicrobial Peptides through Molecular Engineering and Self-Assembly. *Biomacromolecules* **2019**, *20* (3), 1362–1374. https://doi.org/10.1021/acs.biomac.8b01740.

(36) Rodríguez-Cabello, J. C.; Girotti, A.; Ribeiro, A.; Arias, F. J. Synthesis of Genetically

Engineered Protein Polymers (Recombinamers) as an Example of Advanced Self-Assembled Smart Materials. In *Methods in molecular biology (Clifton, N.J.)*; 2012; Vol. 811, pp 17–38. https://doi.org/10.1007/978-1-61779-388-2_2.

(37) Roberts, S.; Dzuricky, M.; Chilkoti, A. Elastin-like Polypeptides as Models of Intrinsically Disordered Proteins. *FEBS Lett.* **2015**, *589* (19PartA), 2477–2486. https://doi.org/10.1016/j.febslet.2015.08.029.

(38) Hassouneh, W.; Christensen, T.; Chilkoti, A. Elastin-like Polypeptides as a Purification Tag for Recombinant Proteins. *Curr. Protoc. Protein Sci.* **2010**, *61* (1), 6.11.1-6.11.16. https://doi.org/10.1002/0471140864.ps0611s61.

(39) Hu, F.; Ke, T.; Li, X.; Mao, P. H.; Jin, X.; Hui, F. L.; Ma, X. D.; Ma, L. X. Expression and Purification of an Antimicrobial Peptide by Fusion with Elastin-like Polypeptides in Escherichia Coli. *Appl. Biochem. Biotechnol.* **2010**, *160* (8), 2377–2387. https://doi.org/10.1007/s12010-009-8850-2.

(40) Sousa, D. A.; Mulder, K. C. L.; Nobre, K. S.; Parachin, N. S.; Franco, O. L. Production of a Polar Fish Antimicrobial Peptide in Escherichia Coli Using an ELP-Intein Tag. *J. Biotechnol.* **2016**, *234*, 83–89. https://doi.org/10.1016/j.jbiotec.2016.07.021.

(41) Da Costa, A.; Machado, R.; Ribeiro, A.; Collins, T.; Thiagarajan, V.; Neves-Petersen, M. T.; Rodriguez-Cabello, J. C.; Gomes, A. C.; Casal, M. Development of Elastin-like Recombinamer Films with Antimicrobial Activity. *Biomacromolecules* **2015**, *16* (2), 625–635. https://doi.org/10.1021/bm5016706.

(42) da Costa, A.; Pereira, A. M.; Gomes, A. C.; Rodriguez-Cabello, J. C.; Casal, M.; Machado,

R. Production of Bioactive Hepcidin by Recombinant DNA Tagging with an Elastin-like Recombinamer. *N. Biotechnol.* **2018**, *46* (25), 45–53. https://doi.org/10.1016/J.NBT.2018.07.001.

(43) Acosta, S.; Quintanilla, L.; Alonso, M.; Aparicio, C.; Rodríguez-Cabello, J. C. Recombinant AMP/Polypeptide Self-Assembled Monolayers with Synergistic Antimicrobial Properties for Bacterial Strains of Medical Relevance. *ACS Biomater. Sci. Eng.* **2019**, *5* (9), 4708–4716. https://doi.org/10.1021/acsbiomaterials.9b00247.

(44) Janib, S. M.; Pastuszka, M.; Aluri, S.; Folchman-Wagner, Z.; Hsueh, P.-Y.; Shi, P.; Yi-An; Cui, H.; Mackay, J. A. A Quantitative Recipe for Engineering Protein Polymer Nanoparticles. *Polym. Chem.* **2014**, *5* (5), 1614–1625. https://doi.org/10.1039/C3PY00537B.

(45) Abdolhosseini, M.; Nandula, S. R.; Song, J.; Hirt, H.; Gorr, S.-U. Lysine Substitutions Convert a Bacterial-Agglutinating Peptide into a Bactericidal Peptide That Retains Anti-Lipopolysaccharide Activity and Low Hemolytic Activity. *Peptides* **2012**, *35* (2), 231–238. https://doi.org/10.1016/j.peptides.2012.03.017.

(46) Mansour, S. C.; de la Fuente-Núñez, C.; Hancock, R. E. W. Peptide IDR-1018: Modulating the Immune System and Targeting Bacterial Biofilms to Treat Antibiotic-Resistant Bacterial Infections. *J. Pept. Sci.* **2015**, *21* (5), 323–329. https://doi.org/10.1002/psc.2708.

(47) Moussa, D. G.; Kirihara, J. A.; Ye, Z.; Fischer, N. G.; Khot, J.; Witthuhn, B. A.; Aparicio, C. Dentin Priming with Amphipathic Antimicrobial Peptides. *J. Dent. Res.* **2019**, *98* (10), 1112–1121. https://doi.org/10.1177/0022034519863772.

(48) Haney, E. F.; Wu, B. (Catherine); Lee, K.; Hilchie, A. L.; Hancock, R. E. W. Aggregation and Its Influence on the Immunomodulatory Activity of Synthetic Innate Defense Regulator Peptides. *Cell Chem. Biol.* **2017**, *24* (8), 969-980.e4. https://doi.org/10.1016/j.chembiol.2017.07.010.

(49) Bahniuk, M. S.; Alshememry, A. K.; Elgersma, S. V.; Unsworth, L. D. Self-Assembly/Disassembly Hysteresis of Nanoparticles Composed of Marginally Soluble, Short Elastin-like Polypeptides. *J. Nanobiotechnology* **2018**, *16* (1), 15. https://doi.org/10.1186/s12951-018-0342-5.

(50) Kuna, M.; Mahdi, F.; Chade, A. R.; Bidwell, G. L. Molecular Size Modulates Pharmacokinetics, Biodistribution, and Renal Deposition of the Drug Delivery Biopolymer Elastin-like Polypeptide. *Sci. Rep.* **2018**, *8* (1), 7923. https://doi.org/10.1038/s41598-018-24897-9.

(51) Woody, R. W. Circular Dichroism of Intrinsically Disordered Proteins. In *Instrumental Analysis of Intrinsically Disordered Proteins*; John Wiley & Sons, Inc.: Hoboken, NJ, USA, 2010; pp 303–321. https://doi.org/10.1002/9780470602614.ch10.

(52) Yamaoka, T.; Tamura, T.; Seto, Y.; Tada, T.; Kunugi, S.; Tirrell, D. A. Mechanism for the Phase Transition of a Genetically Engineered Elastin Model Peptide (VPGIG)40 in Aqueous Solution. *Biomacromolecules* **2003**, *4* (6), 1680–1685. https://doi.org/10.1021/bm034120l.

(53) Quiroz, F. G.; Chilkoti, A. Sequence Heuristics to Encode Phase Behaviour in Intrinsically Disordered Protein Polymers. *Nat. Mater.* **2015**, *14* (11), 1164–1171.

https://doi.org/10.1038/nmat4418.

(54) Ye, Z.; Aparicio, C. Modulation of Supramolecular Self-Assembly of an Antimicrobial Designer Peptide by Single Amino Acid Substitution: Implications on Peptide Activity. *Nanoscale Adv.* **2019**, *1* (12), 4679–4682. https://doi.org/10.1039/C9NA00498J.

(55) Roberts, S.; Miao, V.; Costa, S.; Simon, J.; Kelly, G.; Shah, T.; Zauscher, S.; Chilkoti, A. Complex Microparticle Architectures from Stimuli-Responsive Intrinsically Disordered Proteins. *Nat. Commun.* **2020**, *11* (1), 1–10. https://doi.org/10.1038/s41467-020-15128-9.